IOP PUBLISHING PLASMA PHYSICS AND CONTROLLED FUSION

Plasma Phys. Control. Fusion **50** (2008) 124044 (12pp) doi:10.1088/0741-3335/50/12/124044

Fast-ignition target design and experimental-concept validation on OMEGA

C Stoeckl[1], K S Anderson[1], R Betti[1,2], T R Boehly[1], J A Delettrez[1], J A Frenje[3], V N Goncharov[1], V Yu Glebov[1], J H Kelly[1], A J MacKinnon[4], R L McCrory[1], D D Meyerhofer[1,2], S F B Morse[1], J F Myatt[1], P A Norreys[5], P M Nilson[1], R D Petrasso[3], T C Sangster[1], A A Solodov[1], R B Stephens[6], M Storm[1], W Theobald[1], B Yaakobi[1], L J Waxer[1] and C D Zhou[1]

[1]Laboratory for Laser Energetics, University of Rochester, Rochester, NY 14623, USA
[2] Departments of Mechanical Engineering and Physics and Fusion Science Center, University of Rochester, Rochester, NY 14623, USA
[3] Massachusetts Institute of Technology, Cambridge, MA 02139, USA
[4] Lawrence Livermore National Laboratory, Livermore, CA 94550, USA
[5] Rutherford Appleton Laboratory, Didcot, OX11 0QX, UK
[6] General Atomics, San Diego, CA 92186, USA

Received 29 May 2008, in final form 14 August 2008
Published 5 November 2008
Online at stacks.iop.org/PPCF/50/124044

Abstract

A comprehensive scientific program is being pursued at LLE to explore the physics of fast ignition. The OMEGA EP Laser was completed in April 2008, adjacent to the 60 beam, 30 kJ OMEGA Laser Facility. OMEGA EP consists of four beamlines with a NIF-like architecture, each delivering up to 6.5 kJ of UV laser energy in long pulse (ns) mode into the OMEGA EP target chamber. Two of the beamlines can operate as high-energy petawatt lasers, with up to 2.6 kJ each with 10 ps pulse duration. These beams can either be injected into the OMEGA EP target chamber or combined collinearly into the existing OMEGA target chamber for integrated fast-ignitor experiments. Fuel-assembly experiments on OMEGA have achieved high fuel areal densities, and the effects of a cone on the fuel assembly are being studied. Experiments on short-pulse laser systems in collaboration with other institutions are being pursued to investigate the conversion efficiency from laser energy to fast electrons. A coherent transition radiation diagnostic to study the transport of the electrons in high-density material is being developed. Integrated experiments with room-temperature targets on OMEGA will be performed in 2008. Simulations of these integrated experiments show significant heating of up to 1 keV due to the hot electrons from the short-pulse laser.

(Some figures in this article are in colour only in the electronic version)

1. Introduction

The fast-ignitor concept for inertial confinement fusion [1, 2] has shown significant promise due to successful small-scale integrated experiments [3, 4]. It makes it possible to use lower driver energies than conventional hot-spot ignition [5] and has the potential for higher gains. The fast-ignitor concept separates the fuel assembly and fuel heating by using an ultrafast laser in addition to a driver that compresses the fuel to high density. The ultrafast laser produces relativistic electrons with high efficiency (up to 50% has been reported [6]) that heat the fuel. Compression-driver options include the laser or heavy-ion-beam-heated hohlraums or laser direct drive [7].

Many challenges remain for the fast-ignitor concept. The first is to demonstrate the fuel compression to areal densities required for ignition. The conversion efficiency from ultrafast laser to energetic electrons must be high at ignition-relevant intensities, energies and pulse lengths. The energy distribution of the hot electrons must be compatible with the areal density of the compressed core to ensure that the electrons deposit most of their energy into a hot spot of at least $0.3\,\mathrm{g\,cm^{-2}}$ [8]. Another challenge is the transport of relativistic electrons from the critical-density region ($n_e \sim 10^{21}\,\mathrm{cm^{-3}}$ for a typical 1 μm laser), where the ultrafast laser is absorbed and converted into electrons, to the compressed fuel—a distance that can be hundreds of micrometers in an ignition-scale target. For an electron-beam divergence of $\sim 20^\circ$ the overlap between the electron beam originating from a small focal spot ($\sim 10\,\mu$m radius) and the dense core with a diameter of $<50\,\mu$m would be very small [9, 10]. Two solutions to minimize this standoff distance have been proposed: (1) a channeling beam to bore a hole in the plasma atmosphere around the core [2, 11] that allows the ultrafast laser to be absorbed closer to the core; (2) a re-entrant cone to keep the path of the ultrafast laser free of plasma and bring it as close as possible to the dense core [3, 12]. The cone-in-shell concept, while advantageous with respect to the electron transport, breaks the symmetry of the spherical fuel assembly, which could limit the fuel areal density that can be achieved with a given driver energy. Another issue for cone targets is plasma filling the inside of the cone from the shock wave that the high-pressure core plasma sends through the gold cone, which could significantly increase the electron propagation distance. Self-generated electromagnetic fields from the propagation of the electron beam in plasma will modify both the transport and the energy-deposition characteristics. The transport and energy deposition of the fusion alpha particles in near-ignition plasma conditions could significantly change the plasma conditions in the assembled fuel.

All of these physics areas will be experimentally accessible with the combined OMEGA/OMEGA EP Facility at the University of Rochester's Laboratory for Laser Energetics (LLE). OMEGA EP [13] provides two short-pulse ($\sim$1 ps to 100 ps), high-energy laser beams with an energy of up to 2.6 kJ per beam at 1.053 μm, integrated into the existing OMEGA [14] Laser Facility (60 beam, 30 kJ at 0.35 μm). The OMEGA EP beams can be combined collinearly and coaxially and routed to either the existing OMEGA target chamber or the new OMEGA EP target chamber. The combined beams allow the channeling approach to fast ignition (FI) to be studied under realistic conditions for the first time, whereas only one beam is required for cone-in-shell experiments. The OMEGA/OMEGA EP Facility will be well suited to perform integrated fast-ignition experiments because of OMEGA's unique ability to compress cryogenic D_2 and DT targets [15, 16]. To study alpha transport under realistic conditions, the areal density of the compressed core must be of the order of the hot-spot areal density of an ignition target, $\sim 0.3\,\mathrm{g\,cm^{-2}}$ [8], which could be achieved in high-performance cryogenic-DT implosions on OMEGA [17].

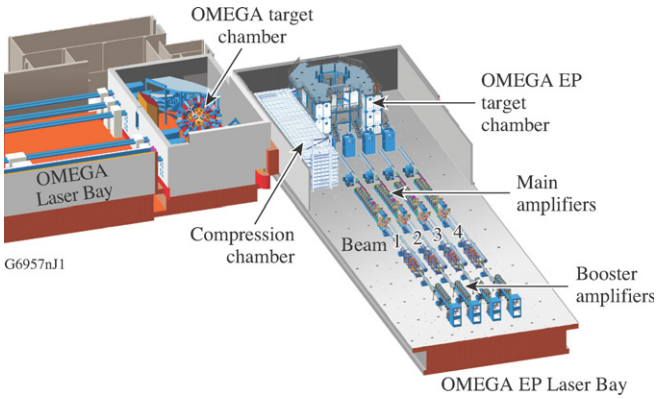

Figure 1. Schematic of the expanded OMEGA facility. The new OMEGA EP laser adjacent to the existing 60-beam OMEGA facility includes four NIF-like beamlines, a compression chamber and a new target chamber. Two of the four beams can be run in short-pulse mode and can be directed into either target chamber. All four beams can be converted into UV and used in the OMEGA EP target chamber.

This manuscript describes several important components of LLE's program to investigate the physics of the fast-ignitor concept. Section 2 introduces the OMEGA/OMEGA EP integrated laser facility. Hydrodynamic experiments on high-areal-density implosion and fuel assembly with cone-in-shell targets are described in section 3. Section 4 discusses experiments to measure the conversion efficiency from laser light into energetic electrons and the development of a coherent transition radiation (CTR) diagnostic to investigate the hot-electron transport. Section 5 summarizes simulations of integrated fast-ignitor physics experiments on OMEGA EP and full-scale, high-gain, fast-ignition experiments. Section 6 provides a short summary.

2. Laser system

The OMEGA EP Laser Facility is housed in a structure on the south side of the existing OMEGA laser building (see figure 1). The OMEGA Laser System delivers up to 30 kJ of UV light in 60 beams, arrayed symmetrically for uniform illumination of spherical implosion targets [14]. OMEGA has a elaborate pulse-shaping system, which can provide up to ∼4 ns long, highly shaped pulses with a contrast of up to 100. The individual OMEGA beams are smoothed by distributed phase plates (DPPs) [18], two-dimensional smoothing by spectral dispersion (SSD) [19] with 1 THz bandwidth in the UV and polarization smoothing (PS) [20].

The four new OMEGA EP beamlines use a folded NIF-like architecture [21]—an upper level that includes a 7-disk booster amplifier and a transport spatial filter, and a lower level that includes an 11-disk main amplifier, a cavity spatial filter, a plasma-electrode Pockels cell (PEPC) [22], and a deformable mirror. A second polarizer is inserted between the PEPC and the cavity spatial filter to protect the laser system against IR light reflected from the target when the beamline is operated in short-pulse mode. Two of the beams can be compressed using four 141 cm × 41 cm diffraction-grating units, with each unit consisting of three multilayer-dielectric grating tiles [23, 24]. A deformable mirror placed after the last grating unit provides further wavefront correction in each beamline. The beams are either combined and propagate coaxially through evacuated tubes to the OMEGA or OMEGA EP target chamber or directed into the OMEGA EP chamber on separate paths in an orthogonal configuration. An $f/2$

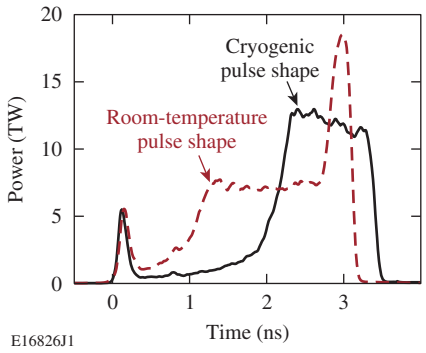

Figure 2. Laser pulse shapes used in the low-adiabat OMEGA cyrogenic (solid) and room-temperature (dashed) target implosions.

off-axis parabola focuses the short-pulse beam to provide a small focal spot even with the expected phase-front distortions in such a large-scale, high-energy laser system. The beams are synchronized to each other and to the OMEGA laser pulse to better-than-10 ps rms. A comprehensive set of laser diagnostics measures the laser energy, pulse duration, and, for the first time on a high-energy petawatt (HEPW) system, the focal-spot intensity distribution at full energy. All four beams can be converted into the third harmonic at 351 nm (<10 ns, up to 6.5 kJ) and used as long-pulse beams in the OMEGA EP target chamber. The long-pulse beams are focused with $f/6.5$ lenses onto the target and are arrayed in a square with a 23° angle to their common centerline. DPPs for beam smoothing will be available in 2009.

3. Fuel-assembly experiments

High fuel compression and high areal densities have been achieved on OMEGA, with both cryogenic targets [25] and room-temperature targets [26], using highly shaped pulses that put the target on a low adiabat (ratio of the shell pressure to the Fermi-degenerate pressure). It has been shown that the areal density ρR depends mostly on the adiabat α of the target and the laser energy E [27]:

$$(\rho R)_{\max} = 2.6/\alpha^{0.54} E_{\mathrm{MJ}}^{0.33}. \tag{1}$$

The cryogenic targets are 10 μm thick, ~430 μm outer-radius CD shells, filled with D_2 to form a 95 μm thick layer at the inside of the CD shell at cryogenic temperatures. The pulse shape for the cryogenic target (figure 2) uses a decaying-shock-adiabat shaping picket [28] and a slowly rising main pulse to put the cryogenic D_2 fuel on an adiabat of $\alpha \sim 2$. The areal density of the imploded targets is inferred from the energy downshift in the secondary-proton spectrum [29]. These protons are created by D^3He fusion reactions, which are secondary reactions in D_2 fuel. Figure 3 shows a measured secondary-proton spectrum from the cryogenic target compared with 1D *LILAC* [30] simulations [25]. An areal density of ~200 mg cm^{-2} can be inferred from the spectrum, which is more than 80% of the clean 1D predictions. The density of the compressed D_2 approaches ~100 g cm^{-3}—a 500-fold compression of the original D_2-ice density.

In the room-temperature experiments, 40 μm thick, 430 μm outer-radius plastic shells coated outside with a 0.1 μm layer of aluminum and filled with D_2 gas with pressures ranging from 8 to 25 atm were imploded using relaxation adiabat shaping, ~16–20 kJ UV laser pulses [31, 32]. A typical experimental pulse shape that puts the room-temperature plastic

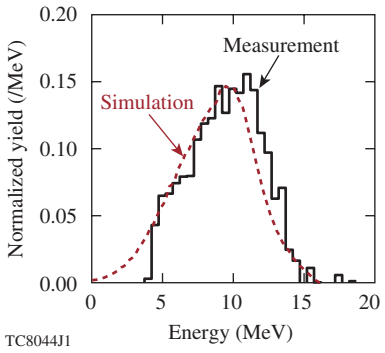

Figure 3. Measured secondary-proton spectrum (solid line) for the cryogenic target. The dashed line shows the calculated spectrum from the 1D hydrocode.

targets on an adiabat of $\alpha \sim 1.5$ is shown in figure 2. A picket at the beginning of the pulse and a spike at the end of the pulse were used to optimize the implosion for high yield and high areal density. The room-temperature targets also showed areal densities of up to $\sim$200 mg cm^{-2} and densities of the order of 100 g cm^{-3}, which translates into a 100-fold compression.

Fuel assembly in cone-in-shell targets has been investigated on OMEGA in both indirect- [33] and direct-drive [34] geometries. Gas-tight targets developed for the direct-drive experiments made it possible to fill the targets with D_2 or D^3He and use nuclear diagnostics to measure the areal density achieved in the implosion. The targets were 24–40 μm thick CH shells of $\sim$870 μm outer diameter a hollow gold cone with an opening angle of 70°or 35° was inserted through a hole in the shell [34]. A shelf on the cone defines the distance between the cone tip and the center of the shell, typically 30 ± 10 μm. The cone has a thickness of $\sim$100 μm outside the shell and 10 μm inside the shell and ends in a 30 μm thick hyperbolic-shaped tip. For some experiments the cone tip was cut off to form a 15 μm thick flat tip. Most experiments used 54 of the 60 OMEGA beams, at 351 nm wavelength, with a 1 ns square pulse and $\sim$21 kJ of total energy or a highly shaped pulse of $\sim$3 ns duration and $\sim$20 kJ energy. For some experiments, 15 beams with a total energy of $\sim$6 kJ were diverted to a backlighter foil. The target was irradiated using 35 of the remaining beams with $\sim$11 kJ of laser energy.

X-ray framing cameras [35] were used to acquire backlit images of the fuel assembly around the cone tip. Figure 4 shows a backlit image of a cone-in-shell target (lower half) irradiated with a 1 ns square pulse at peak density compared with a 2D *DRACO* [36] hydrodynamic simulation (upper half). The image shows a dense core $\sim$100 μm from the cone tip, with lower-density plasma in between. These features can also be seen in the *DRACO* simulation; only the reaction of the cone tip looks qualitatively different. The cone tip seems to be crushed on axis in the simulations, whereas it looks like it is pushed away from the core in the experimental images [34]. An areal density of $\sim$70 mg cm^{-2} was measured for a 35° cone target using nuclear diagnostics—more than 60% of what a 1D simulation predicts for an equivalent full sphere [34]. Mixing does not seem to be an issue in these direct-drive cone experiments [34].

A streaked optical pyrometer (SOP) [37] was used to investigate the filling of the inside of the cone. The SOP uses an optical system that images the inside of the tip of the cone onto the slit of the streak camera with an $\sim$10 μm spatial resolution and a 500 μm field of view. The breakout of the shock produces a short burst of light that is recorded on the streak camera.

Figure 5 shows a lineout through the center of the SOP trace from a 35° cone target with a 15 μm thick flat tip irradiated by a highly shaped pulse at 20 kJ energy, as well as the areal

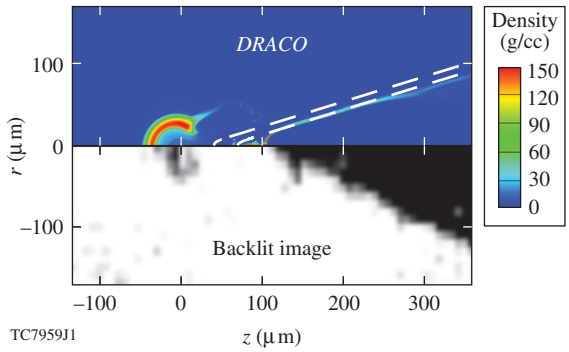

Figure 4. Backlit framing-camera image from a target filled with 10 atm of D_2 and imploded using a 1 ns square pulse at 11 kJ laser energy, compared with a 2D *DRACO* radiation hydrodynamic-code simulation.

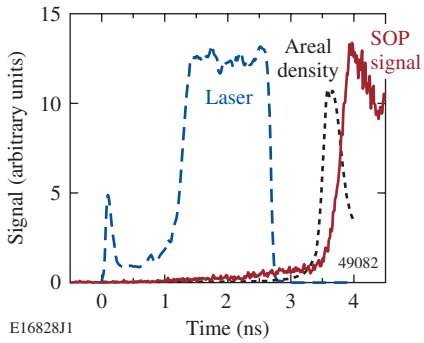

Figure 5. Lineout through the center of the SOP signal (solid line) of a cone-in-shell target with a 35° opening angle irradiated with a shaped pulse at 20 kJ. The dashed line shows the laser pulse power and the dotted line represents the calculated evolution of the areal density.

density of the compressed core as predicted by the 2D hydrocode *DRACO* and the drive-laser pulse shape. The shock signal starts just after the time of peak compression as calculated by *DRACO*. The absolute timing uncertainty of the SOP is estimated to be ∼100 ps. With the current target designs the inside of the cone is free of plasma at the time when the short-pulse laser would propagate. Since the projected range for a 1 MeV electron in gold is of the order of ∼50 μm [38], the gold tip must be as thin as possible to avoid excessive energy loss of the fast electrons.

4. Short-pulse experiments and diagnostics

The conversion efficiency from laser energy into energetic electrons $\eta_{L\to e}$ has been measured using K-shell spectroscopy of reduced-mass Cu targets [39]. It has been shown that the fast-electron-induced K_α yield from reduced-mass targets can be readily used to infer $\eta_{L\to e}$ [40, 41]. The heating of these reduced-mass targets is sufficient to affect the inner-shell fluorescence probabilities [41]. Ionization of the outer shells of copper at high temperature affects the M→K and the L→K transition probabilities and causes a deviation in the ratio of the emitted number of K_β and K_α photons. This is used to infer the electron temperature of the target and the conversion efficiency $\eta_{L\to e}$ independently from the absolute K_α yield [41].

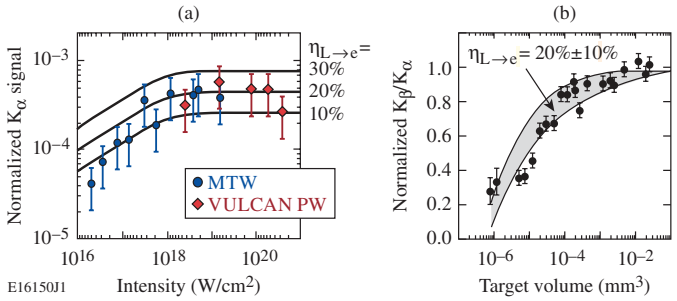

Figure 6. (*a*) Energy in K_α photons (normalized to the laser energy) emitted by a $500\times500\times20\ \mu m^3$ copper target as a function of laser intensity. The curves correspond to the total calculated K_α yield at a given laser-to-electron-energy-conversion efficiency $\eta_{L\to e}$. (*b*) Ratio of the number of K_β to K_α photons (normalized to the cold-material value) as a function of target volume. Numerical calculations of K_β/K_α are shown as a function of target volume caused by target heating, assuming $\eta_{L\to e} = 20 \pm 10\%$.

These experiments have been performed on both the Rutherford Appleton Laboratory PW facility [42] and the multi-terawatt (MTW) laser at LLE [43]. The Vulcan PW laser delivers up to 500 J of energy with a pulse duration as short as 0.5 ps at a wavelength of 1.054 μm, focused using an $f/3$ off-axis parabola onto the target. Roughly 30% of the laser energy is contained in a 7 μm full-width-at-half-maximum (FWHM) spot. The MTW laser delivered 1–5 J, 1 ps pulses at a wavelength of 1.054 μm and was focused using an $f/2$ off-axis parabola. The focal spot has an FWHM of ~5 μm containing ~50% of the laser energy. Copper foils ranging between $20 \times 20 \times 2\ \mu m^3$ and $500 \times 500 \times 50\ \mu m^3$ were used as targets. The K-shell line radiation was measured using a single-photon-counting spectrometer [44], based on an SI 800–145 x-ray back-illuminated, charge-coupled device (CCD) [45]. Figure 6 [39] shows the measured conversion efficiency of laser energy into K_α photons emitted from $500\times500\times20\ \mu m^3$ copper targets as a function of the laser intensity. The K_α photon yield increases up to intensities of 10^{18} W cm^{-2} and stays constant at higher intensity. The data from figure 6 are compared with a model of K_α photon production, which assumes an exponentially distributed fast-electron spectrum $f(E) = \exp(-E/T_e)$, where T_e is calculated from the laser intensity through the ponderomotive scaling [46]:

$$T_e(\text{MeV}) = 0.511[(1 + I_{18}\lambda^2_{\mu m}/1.37)^{0.5} - 1], \tag{2}$$

where E is the electron energy, T_e is the electron temperature, I_{18} is the laser intensity in units of 10^{18} W cm^2 and $\lambda_{\mu m}$ is the laser wavelength in micrometers. The energy loss of the fast electrons is calculated using a continuous-slowing-down approximation for cold, solid-density copper.

The model assumes that all electrons are reflected at the target boundaries from electrostatic sheath fields [47, 48] and deposit all their energy in the target (refluxing). Relativistic corrections to the copper K-shell ionization cross section [49] are included, and the only free parameter in the model is the conversion efficiency $\eta_{L\to e}$. A laser-to-electron-energy-conversion efficiency $\eta_{L\to e} = (20 \pm 10)\%$ can be inferred by comparing the experimental data with the predictions of this model. The discrepancies in the observed K_α yield at lower laser intensities are most likely due to the assumption of ponderomotive scaling that breaks down at intensities below 10^{18} W cm^{-2} [46].

Figure 6(*b*) [39] shows measurements of the change in the ratio of the number of emitted K_β and K_α photons (K_β/K_α) normalized to the cold-material value as a function of the

target volume at a constant laser intensity of $2 \times 10^{19}\,\mathrm{W\,cm^{-2}}$. Numerical target-heating calculations using the implicit-hybrid particle-in-cell code *LSP* [50] infer the energy content of the fast electrons from the reduction the ratio of K_β/K_α [41]. The collisional–radiative code PrismSPECT [51] was used to determine the target ion-population distribution. Assuming a conversion efficiency of $\eta_{L\to e} = (20 \pm 10)\%$, the calculation reproduces the observed variation in the ratio K_β/K_α with target volume, which is consistent with the efficiencies inferred from the absolute K_α yield. Both techniques can be readily extended to laser energies on the multi-kilojoule level and pulse durations $>10\,\mathrm{ps}$ on OMEGA EP, much closer to the fast-ignitor laser conditions as in the present small-scale experiments.

A promising technique that provides information about the transport of the energetic electrons generated in the short-pulse laser–plasma interaction is the measurement of transition radiation (TR) [52]. TR is emitted when a charged particle passes through a refractive-index interface [53]—in this case, energetic electrons exiting the target into vacuum. The emitted electromagnetic energy is very small for a single electron. However, the laser-generated energetic-electron distribution typically has a highly correlated temporal electron-density structure, which leads to a considerable coherent enhancement producing CTR [54]. The two dominant electron-acceleration processes produce structures at different frequencies: resonance absorption [55] accelerates electrons into the target once every optical cycle creating a CTR signal at the first harmonic of the laser frequency, whereas the $\vec{v} \times \vec{B}$ force [46] accelerates electrons twice every optical cycle, generating a CTR signal at the second harmonic. The spatial-intensity distribution and spectrum of the CTR emission measured at the backside of the target provide information about the electron transport, especially the electron spatial distribution, divergence and the slope or temperature of the electron energy distribution.

A transition radiation diagnostic (TRD) [56] has been developed to acquire high-resolution images of the target's rear-side optical emission at the second harmonic ($\lambda \sim 527\,\mathrm{nm}$) for experiments conducted on the MTW laser. This instrument uses a commercial 20× infinity corrected objective [57] to collect the optical emission from the target's rear surface. An optical system of three 200 mm focal length achromatic lenses and a 50/50 beam splitter transports the light to a CCD camera. A separate optical system is used to position the microscope objective with $\sim 1\,\mu\mathrm{m}$ precision relative to the rear surface of the target since its depth of focus is only $1.6\,\mu\mathrm{m}$. Extensive tests have shown that the optical resolution of the TRD in the optimum focus position is limited only by the CCD pixel size to $\sim 1.4\,\mu\mathrm{m}$ over the full field of view [56]. Background signals are minimized by folding the optical system through 90° so that the detector can be shielded with lead from direct and scattered hard x-rays. This shielding reduces the background by more than an order of magnitude [56].

The TRD has been used in several experiments to diagnose electron transport in solid materials. Figure 7 shows a CTR image from the rear side of a $30\,\mu\mathrm{m}$ thick aluminum foil. A 5 J, 500 fs pulse from the MTW laser was focused to an $\sim 4\,\mu\mathrm{m}$ radius spot on the target, corresponding to a laser intensity of $\sim 10^{19}\,\mathrm{W\,cm^{-2}}$. The diameter of the rear-side coherent optical emission is less than $20\,\mu\mathrm{m}$. Small structures are clearly visible in this region with a spatial FWHM of $\sim 2\,\mu\mathrm{m}$, superimposed on a ring-like feature. These structures are indicative of electron-beam filamentation [58].

This instrument will be used extensively to study the divergence and potential breakup of the electron flow through the target and to infer the slope temperature of the energetic electrons [54]. Based on the experience with this TRD on the MTW, a detector suitable for OMEGA EP is being designed.

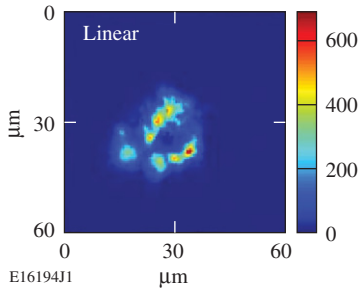

Figure 7. Image of the rear-side optical CTR emission from a 30 μm thick aluminum foil. The color scale is linear and the intensity is expressed in arbitrary units. A number of ~2 μm diameter filaments are contained within a 20 μm diameter emission region.

5. Simulations

To understand the interaction of the electron beam with the target and its effect on the neutron production in both integrated FI experiments on OMEGA EP and high-gain FI targets, the 2D axisymmetric radiation hydrocode *DRACO* [36] was coupled with the 2D/3D hybrid-PIC code *LSP* [50]. *DRACO* simulates the target implosion and the hydrodynamic reaction of the target to the fast-electron heating, including all relevant physics, with the exception of radiation transport, using a multi-material piece-wise parabolic method (PPM) and a Eulerian hydrodynamic scheme with a moving grid in spherical geometry, along with SESAME equation of state and flux-limited thermal conduction [36]. The capsule was driven by a uniform, quasi-1D (see [36]) laser illumination on the surface of the capsule (no laser illumination on the cone). No boundary approximations were made at either cone surface. *LSP* is used to simulate the hot-electron transport, including self-generated electromagnetic fields. The laser–plasma interaction that creates the energetic electrons is not modeled in *LSP*; a hot-electron distribution is created by promoting background electrons to higher energy according to a theoretical prescription such as Wilks's scaling law [46] and a constant conversion efficiency. The transport of hot electrons is currently modeled in *LSP* only from the end of the cone tip for cone-in-shell targets to the dense core, where the hot-electron energy is absorbed; the cone itself and the electron transport in the cone are not simulated.

The *LSP* part of the simulation starts when the high-energy, short-pulse laser is injected using the hydrodynamic profiles predicted by *DRACO*. *LSP* runs for a short time (~1 ps) during which the hydrodynamic evolution is minimal and it generates a time history of hot-electron energy deposition. *DRACO* then runs for the same time using the energy deposition calculated by *LSP* as an additional energy source in the temperature equation. The hydrodynamic profiles in *LSP* are updated according to the *DRACO* results, while the hot-electron distributions and the electromagnetic fields in *LSP* are left unchanged. *DRACO* and *LSP* are run together for the duration of the HEPW pulse. The hydrodynamic reaction of the target after the HEPW pulse is simulated by *DRACO*.

The first simulations of integrated fast-ignitor experiments planned for the combined OMEGA/OMEGA EP Laser System used 40 μm thick CD shells of ~870 μm outer diameter, a gold cone with an opening angle of 35° and a tip thickness of 15 μm, irradiated by a highly shaped laser pulse of ~3 ns duration and ~20 kJ energy. Currently, radiation transport is not included in the hydro simulation, which leads to an overestimate of the compressed target density. OMEGA EP is assumed to deliver 2.6 kJ in a 10 ps pulse into the cone, which is translated into a hot-electron distribution assuming a 30% conversion efficiency and a slope

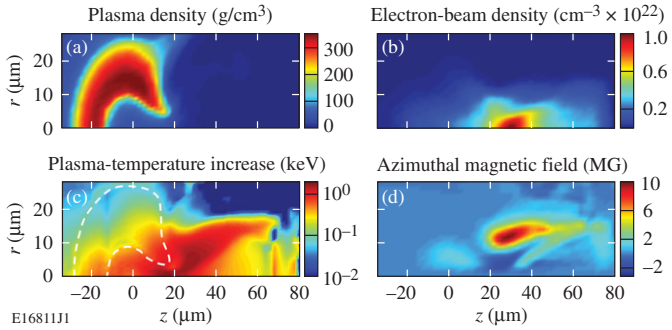

Figure 8. Snapshots of the (*a*) plasma density, (*b*) hot-electron density, (*d*) the azimuthal magnetic field 6 ps after the beginning of the hot-electron pulse, for near-term integrated fast-ignitor experiments on OMEGA. The maximum increase in plasma temperature (*c*) at the end of the pulse is of the order of 1 keV.

temperature according the Wilks scaling. The hot electrons are given a Gaussian profile in the radial direction with a diameter of 20 μm (FWHM) and an angular spread of 20° (half-angle, FWHM). Figure 8 shows results from these simulations as 2D maps of (*a*) the plasma density, (*b*) hot-electron density, and (*d*) the azimuthal magnetic field in the r–z plane 6 ps after the beginning of the hot-electron pulse. Figure 8(*c*) shows the total plasma temperature increase caused by the heating by hot electrons at the end of laser pulse, with a maximum of ∼1 keV. The hot electrons are seen to be well collimated by the resistive magnetic field generated by the electron beam despite the high initial divergence.

This *LSP*/*DRACO* code combination scheme was also used to perform integrated high-gain, fast-ignition simulations. An optimized spherically symmetric target imploded with a highly shaped 300 kJ compression pulse [7] was used and the electron beam was injected 125 μm from the target center. The electron beam had a square profile in time with a duration of 10 ps and a Gaussian profile in the radial direction with a diameter of 30 μm (FWHM). A Maxwellian distribution was assumed for the electrons with a mean energy of 2 MeV and an angular spread of 20° (half-angle, FWHM). For the given parameters, 43 kJ of energetic electrons were required for ignition, resulting in a gain of ∼100. When the effect of the magnetic field on beam electrons was artificially suppressed, the minimum electron-beam energy required for ignition increased to 96 kJ, demonstrating the beneficial effect of the resistive magnetic field.

6. Summary

A comprehensive scientific program is being pursued at LLE to investigate the fast-ignitor concept for inertial confinement fusion. The combined OMEGA/OMEGA EP Laser Facility provides the experimental infrastructure for these investigations. The OMEGA EP laser was completed in April 2008 and provides two short-pulse beamlines with up to 2.6 kJ each with 10 ps pulse duration. These beams can be routed into either the OMEGA EP chamber or combined collinearly into the existing OMEGA target chamber for integrated fast-ignitor experiments. Fuel-assembly experiments on OMEGA with both room-temperature and cryogenic targets have achieved high fuel areal densities of ∼200 mg cm^{-2}, sufficient to stop the MeV electrons produced by the short-pulse laser. Experiments on the fuel assembly of cone-in-shell targets showed only a small deterioration of achievable areal density. The measured areal

density was more than 60% of what a 1D simulation predicts for an equivalent full sphere. The conversion efficiency from laser energy to fast electrons was measured using two independent experimental methods on both LLE's MTW laser and the RAL Vulcan Petawatt and found to be ∼20% at intensities $>10^{18}\,\mathrm{W\,cm^{-2}}$. A high-resolution (1.4 μm) TRD measures the CTR from the rear side of a solid target, providing insight into the hot-electron transport. Simulations of both full-scale fast-ignition experiments and near-term integrated experiments on OMEGA, using a combination of radiation hydrocode (*DRACO*) and a hybrid particle-in-cell code (*LSP*), show the beneficial effects of the resistive magnetic fields generated by the propagation of the energetic electron into the high-density core. A decrease in the energy required to ignite a target imploded by a 300 kJ UV laser from ∼100 kJ electron energy to ∼40 kJ electron energy due to the magnetic fields was observed in simulations of full-scale fast-ignition targets. Simulations of fast-ignitor experiments with room-temperature cone-in-shell targets on OMEGA EP showed a temperature increase of up to 1 keV with the short-pulse-laser-produced energetic electrons heating the target. Integrated experiments with room-temperature targets on the combined OMEGA/OMEGA EP facility are scheduled for 2008.

Acknowledgments

This work was supported by the US Department of Energy Office of Inertial Confinement Fusion under Cooperative Agreement No DE-FC52-08NA28302, Fusion Science Center, Office of Inertial Fusion Energy Science No DE-FC02-ER54789, the University of Rochester, and the New York State Energy Research and Development Authority. The support of DOE does not constitute an endorsement by DOE of the views expressed in this paper.

References

[1] Basov N G, Gus'kov S Y and Feokistov L P 1992 *J. Sov. Laser Res.* **13** 396–99
[2] Tabak M *et al* 1994 *Phys. Plasmas* **1** 1626–34
[3] Kodama R *et al* 2001 *Nature* **412** 798–802
[4] Kodama R *et al* 2002 *Nature* **418** 933–34
[5] Lindl J D, McCrory R L and Campbell E M 1992 *Phys. Today* **45** 32–40
[6] Yasuike K *et al* 2001 *Rev. Sci. Instrum.* **72** 1236–40
[7] Betti R *et al* 2005 *Phys. Plasmas* **12** 042703
[8] Nuckolls J *et al* 1972 *Nature* **239** 139
[9] Li C K and Petrasso R D 2004 *Phys. Rev.* E **70** 067401
[10] Stephens R B *et al* 2004 *Phys. Rev.* E **69** 066414
[11] Kitagawa Y *et al* 2002 *Phys. Plasmas* **9** 2202–07
[12] Norreys P A *et al* 2000 *Phys. Plasmas* **7** 3721–26
[13] Waxer L J *et al* 2005 *Opt. Photonics News* **16** 30–6
[14] Boehly T R *et al* 1997 *Opt. Commun.* **133** 495–506
[15] Stoeckl C *et al* 2002 *Phys. Plasmas* **9** 2195–201
[16] Sangster T C *et al* 2007 *Phys. Plasmas* **14** 058101
[17] McKenty P W *et al* 2001 *Phys. Plasmas* **8** 2315–22
[18] Lin Y, Kessler T J and Lawrence G N 1996 *Opt. Lett.* **21** 1703–5
[19] Skupsky S and Craxton R S 1999 *Phys. Plasmas* **6** 2157–63
[20] Boehly T R *et al* 1999 *J. Appl. Phys.* **85** 3444–7
[21] Miller G H, Moses E I and Wuest C R 2004 *Opt. Eng.* **43** 2841–53
[22] Rhodes M A *et al* 1995 *Appl. Opt.* **34** 5312–25
[23] Shore B W *et al* 1997 *J. Opt. Soc. Am.* A **14** 1124–36
[24] Kessler T J *et al* 2004 *Opt. Lett.* **29** 635–37
[25] Sangster T C *et al* 2008 *Phys. Rev. Lett.* **100** 185006
[26] Theobald W *et al* 2008 *Phys. Plasmas* **15** 056306
[27] Goncharov V N *et al* 2008 *Phys. Plasmas* **15** 056310

[28] Goncharov V N *et al* 2003 *Phys. Plasmas* **10** 1906–18
[29] Li C K *et al* 2000 *Phys. Plasmas* **7** 2578–84
[30] Delettrez J *et al* 1987 *Phys. Rev.* A **36** 3926–34
[31] Anderson K and Betti R 2004 *Phys. Plasmas* **11** 5–8
[32] Zhou C D *et al* 2007 *Phys. Rev. Lett.* **98** 025004
[33] Stephens R B *et al* 2003 *Phys. Rev. Lett.* **91** 185001
[34] Stoeckl C *et al* 2007 *Phys. Plasmas* **14** 112702
[35] Bradley D K *et al* 1995 *Rev. Sci. Instrum.* **66** 716–18
[36] Radha P B *et al* 2005 *Phys. Plasmas* **12** 056307
[37] Oertel J A *et al* 1999 *Rev. Sci. Instrum.* **70** 803–05
[38] Gupta P K *et al* 1981 *Appl. Phys. Lett.* **39** 32–34
[39] Nilson P M *et al* 2008 *Phys. Plasmas* **15** 056308
[40] Theobald W *et al* 2006 *Phys. Plasmas* **13** 043102
[41] Myatt J *et al* 2007 *Phys. Plasmas* **14** 056301
[42] Danson C N *et al* 2004 *Nucl. Fusion* **44** S239–46
[43] Bagnoud V *et al* 2005 *Opt. Lett.* **30** 1843–45
[44] Stoeckl C *et al* 2004 *Rev. Sci. Instrum.* **75** 3705–07
[45] Spectral Instruments, Tucson, AZ 85745, USA
[46] Wilks S C *et al* 1992 *Phys. Rev. Lett.* **69** 1383–86
[47] Mackinnion A J *et al* 2002 *Phys. Rev. Lett.* **88** 215006
[48] Sentoku Y *et al* 2003 *Phys. Rev. Lett.* **90** 155001
[49] Kolbenstvedt H 1967 *J. Appl. Phys.* **38** 4785–7
[50] Welch D R *et al* 2001 *Nucl. Instrum. Methods Phys. Res.* A **464** 134–9
[51] Prism Computational Sciences Inc. 455 Science Drive, Madison, WI 53711, USA
[52] Baton S D *et al* 2003 *Phys. Rev. Lett.* **91** 105001
[53] Ginzburg V L 1996 *Phys.—Usp.* **39** 973–82
[54] Zheng J *et al* 2003 *Phys. Plasmas* **10** 2994–3003
[55] Kruer W L 2003 *The Physics of Laser Plasma Interactions* (*Frontiers in Physics*) (Boulder, CO: Westview Press) pp 39–43
[56] Storm M *et al* 2008 *Rev. Sci. Instrum.* at press
[57] Miyamoto K 1989 *Plasma Physics for Nuclear Fusion* Revised (Cambridge, MA: MIT Press)
[58] Gremillet L, Bonnaud G and Amiranoff F 2002 *Phys. Plasmas* **9** 941–48